

Full Length Article

High quality optically active and integrable EuOOH films prepared by pulsed laser deposition

A. Caño^a, B. Galiana^b, G.B. Perea^b, A. de Andrés^c, A. Mariscal-Jiménez^d, J. Gonzalo^a, R. Serna^{a,*}^a Laser Processing Group, Instituto de Óptica, IO-CSIC, Serrano 121, 28006 Madrid, Spain^b Department of Physics, Escuela Politécnica Superior, Universidad Carlos III, 28911 Leganés, Madrid, Spain^c Instituto de Ciencia de Materiales de Madrid, ICM-CSIC, Cantoblanco, 28049 Madrid, Spain^d Department of Applied Physics, Universidad Autónoma de Madrid, C/Francisco Tomás y Valiente 7, 28049 Madrid, Spain

ARTICLE INFO

Keywords:

Thin films

Pulsed laser deposition

Oxyhydroxides

Raman spectroscopy

Rare-earths

Optical properties

ABSTRACT

Rare-earth (RE)-Oxygen-Hydrogen compounds are versatile materials whose composition and properties can be significantly varied by changing the relative O and H contents. Among them hydrides and oxyhydrides have been thoroughly investigated due to its photochromic properties. Instead, research of RE-hydroxides and oxyhydroxides (RE-OH and RE-OOH) is scarce although they show promising properties as light emitters. However, their use and integration in solid state devices have been hindered so far because their usual chemical synthesis routes yield materials in bulk or powder configurations. In this work we demonstrate a physical deposition route based on pulsed laser deposition that results in the unprecedented preparation of high-quality Eu oxyhydroxide (EuOOH) thin films. The synthesized EuOOH films show a well-defined monoclinic structure, are optically active and show a robust red emission related to the intra-f transitions of the Eu^{3+} ions. The excellent quality of these crystalline films has allowed us to obtain relevant properties of the monoclinic EuOOH phase not previously reported such as its refractive index and its Raman spectrum, including the identification of the characteristic phonon modes. These novel EuOOH films have been prepared both on Si and fused silica substrates, and thus are ready for potential integration in solid state optoelectronic components and devices.

1. Introduction

Rare-earth based luminescent compounds are appealing due to their robust light emission based on intra-f electronic transitions that are characterized by monochromatic light emission with well-defined emission bands, long luminescent lifetimes and large Stokes shift.[1] Therefore, these optically active materials have found applications in different technological areas such as in optoelectronics, where they are included in solid state devices as part of integrated optical amplifiers, as phosphorus for white light emission diodes (LEDs), flat emission displays, X-ray detection and anti-counterfeiting.[2–7] In biology and biomedical applications they have been studied for their use in luminescent labels, probes, thermometry and sensors for in vitro and in vivo imaging.[8–14] or for catalysis applications.[15] Among them, metal (M) and in particular rare-earth (RE)-Oxygen-Hydrogen compounds have recently attracted an increasing interest because they are versatile materials whose composition can be varied by changing the relative O

and H contents, thus endowing them with high potential for functional design.[9,16] In this context, Europium-doped metal hydroxides (MOH) and oxyhydroxides (MOOH) have been studied, and Eu^{3+} -related emission within these compounds has been reported.[7,9,17–19] Although the doping procedure has led to successful results, the amount of active Eu ions that can be incorporated is limited by the solubility of the rare-earth ion in the host. Moreover, to achieve an efficient luminescent emission it is important to avoid clustering of the ions within the host, which can lead to the formation of metallic non-active Eu ion clusters. A strategy to avoid these ion clustering problems when doping a host compound is to directly use an Eu-based compound so that the Eu ions are effectively dispersed and well located at the lattice positions. In particular, Eu oxides and hydroxides in bulk (ceramics), films and nanostructures (nanorods and nanoparticles) have demonstrated to provide efficient and even tunable white light emission.[5,20–23] In this work, we follow the above-mentioned path (Eu-based compounds), and we report the successful emission of Eu ions within Eu-oxyhydroxide

* Corresponding author.

E-mail address: rosalia.serna@csic.es (R. Serna).<https://doi.org/10.1016/j.apsusc.2023.158236>

Received 30 March 2023; Received in revised form 18 July 2023; Accepted 10 August 2023

Available online 13 August 2023

0169-4332/© 2023 The Authors. Published by Elsevier B.V. This is an open access article under the CC BY license (<http://creativecommons.org/licenses/by/4.0/>).

thin films prepared by a physical deposition methodology. It should be noted that the main synthesis route for the production of hydroxides and oxyhydroxides is based in chemistry hydrothermal methods, which yield powders and micro-crystals. Furthermore, these methods require several synthesis steps, in which the EuOOH is obtained by $\text{Eu}(\text{OH})_3$ dehydration after thermal annealing at temperatures in the range 225–325 °C. [23–26] In contrast, we propose in this work a facile method for the production of the monoclinic EuOOH phase involving lower annealing temperatures that yields thin solid films on Si-based substrates compatible with CMOS technology, and therefore, suitable for integration in photonic solid state devices. We anticipate that this facile method for fabrication of the EuOOH will be also useful to develop functional luminescent materials for biomedical applications. [9,12,27].

To prepare the EuOOH films we have used pulsed laser deposition (PLD), since plasma deposition methods such as PLD and sputtering are particularly suitable for the deposition of thin films with high density and good optical properties, and both allow doping and reactive processes. [7,22,28,29] In particular, concerning the preparation of RE-Oxygen-Hydrogen compounds Colombi *et al.* demonstrated the fabrication of RE (Sc, Y, Gd) hydrides and oxyhydrides by sputtering for the development of photochromic films, [30] while we have recently reported the preparation by PLD of nanocrystalline Europium oxide (EuO_x , $1 \leq x < 1.4$) thin films with a tunable oxygen stoichiometry and photoluminescence emission. [16] This achievement is based on the unique characteristic of PLD that enables the deposition of thin films in a broad range of background pressures. [22,28,31,32] In this work we profit of this property to achieve the successful formation of Eu-oxyhydroxide (EuOOH) thin films. Moreover, we provide a full description of the novel EuOOH films including microstructure, stability, optical (refractive index) and light emission properties. To our knowledge we report for the first time a full Raman spectrum with information on the phonon modes of the monoclinic EuOOH phase. We believe that this information is essential to promote the use of EuOOH and other RE-oxyhydroxides and related compounds for promising applications in photonics.

2. Methods / experimental

2.1. Thin film preparation

Thin films were prepared by PLD using an ArF excimer laser ($\lambda = 193$ nm, 20 ns pulse duration) at a 10 Hz repetition rate with an energy density of 1.5 J/cm². The laser beam was focused on the surface of a high-purity (99.99%) ceramic Eu_2O_3 target [20] located in a vacuum chamber. The target was rotated during deposition to optimize material extraction. The background pressure in the chamber during film growth was intentionally varied from 9×10^{-2} to 3×10^{-5} Pa in order to study its influence on EuOOH formation. We used an on-axis deposition configuration with the substrates placed in front of the target at a distance of 2.5 cm. Films with a nominal thickness of 100 ± 5 nm were grown at room temperature simultaneously on chemically cleaned polished Si (100) wafers, IR-grade fused silica substrates and carbon coated mica (C-mica) substrates to facilitate their characterization with different techniques. After deposition, the resulting EuO_x films were annealed in air up to 250 °C to induce first the Eu oxyhydroxide formation, and finally up to 450 °C for the decomposition of EuOOH to form the cubic Eu_2O_3 reference film.

2.2. Structural and optical characterization

The film surface morphology was analyzed by a Nikon Eclipse Ti optical microscope (OM) using monochromatic light illumination at 460 nm to enhance the structure. The images have been acquired in reflected light mode with a 100x objective and coupled with a 1.5x Barlow lens. The films deposited on C-mica substrates were floated on deionized water and picked up on a copper TEM-grid for transmission electron microscopy (TEM) analysis. The observation was performed in

a Philips Tecnai 20F FEG at 200 kV. Selected area electron diffraction (SAED) measurements were carried out to determine the microcrystals structure. The crystalline structure of the films was further assessed using X-ray diffraction (XRD) analysis. This was carried out with Co K α radiation in a Bruker AXS D8 diffractometer in grazing incidence condition, with a beam incidence angle of 5° and 2 θ scan between 10 and 120° with a step size of 0.03° over the surface. Subsequently, the Co K α radiation data were converted to Cu K α radiation data in order to standardize the measurements.

The linear optical properties (refractive index and absorption coefficient) of the films were determined at each annealing stage by variable angle ellipsometry. Measurements were performed with a Woollam VASE ellipsometer equipped with a compensator at room temperature in the range of 0.7 to 4.5 eV (1800 to 275 nm) with a 0.05 eV step at angles of incidence (AOIs) of 65°, 70° and 75°. The collected data were analyzed with the WVASE software. Transmission measurements in the infrared range of 2300–3200 nm were performed with a Varian Cary 5000 double-beam spectrophotometer at room temperature in samples deposited on fused silica substrates.

Micro-Photoluminescence (Micro-PL) and Micro-Raman measurements were performed at room temperature exciting with a 488 nm line of Ar⁺ laser with an incident power of 7 mW focused by an Olympus microscope (100x objective). The scattered light is collected and filtered with a “super-notch-plus” filter from Kaiser and analyzed with a Horiba iHR-320 monochromator with an 1800 g/mm grating and a Peltier cooled Synapse CCD detector. The analysis was performed for films deposited on fused silica substrates, and the Raman signals corresponding to the substrates have been subtracted so that the Raman spectrum from the studied films is clearly visualized.

3. Results and discussion

Fig. 1 shows optical microscopy images corresponding to as-deposited and annealed films at 250 °C for 3 h in air and prepared under three different background pressures (9.3×10^{-2} Pa, 8.0×10^{-4} Pa and 3.4×10^{-5} Pa). As-deposited samples show no surface morphology, regardless of the background pressure (Fig. 1 A,C,E). This is consistent with our previous studies that show the formation of amorphous EuO_x films under similar experimental conditions. [5,21] However, the observed morphologies significantly differ after annealing. While the film deposited at 9.3×10^{-2} Pa (Fig. 1B) retains the featureless morphology, films prepared under high vacuum conditions (8.0×10^{-4} and 3.4×10^{-5} Pa, Fig. 1 D,F) show large areas covered with star morphologies with in-plane dimensions ranging from 1 to 10 μm . The high aspect ratio of these stars should be noted, since the film thickness is only 100 nm, whereas their characteristic in-plane dimension is several micrometers. From the images shown in Fig. 1 it can be observed that the characteristic star size decreases and their coverage increases for the highest vacuum pressure (3.4×10^{-5} Pa, Fig. 1F). The increase of the annealing time leads to a complete transformation of the films, as it is shown in supplementary Figure S1 for a film deposited on Si annealed at 250 °C for 3 h.

In order to determine the crystalline character of the stars and their structure, we have combined TEM with XRD analysis for the annealed films. Fig. 2 shows a TEM image of a 10 μm -size isolated star that is representative of the crystallization of the films upon annealing. It shows a 6-pointed star shape with a dendritic pattern (Fig. 2A). Selected area electron diffraction (SAED) pattern, shown in Fig. 2B, confirms the polycrystalline structure of the stars, whereas SAED patterns obtained outside the crystal reveals an amorphous structure, consistent with a non-transformed area of the film. The analysis of the diffraction spots seen in the SAED pattern of Fig. 2B allowed the calculation of the crystal lattice parameters, which are included on Table 1.

The lattice parameters obtained in this work from SAED patterns are in good agreement with those of EuOOH monoclinic structure and the P2₁/m space group, [34,38] which is represented in a scheme in Fig. 2C.

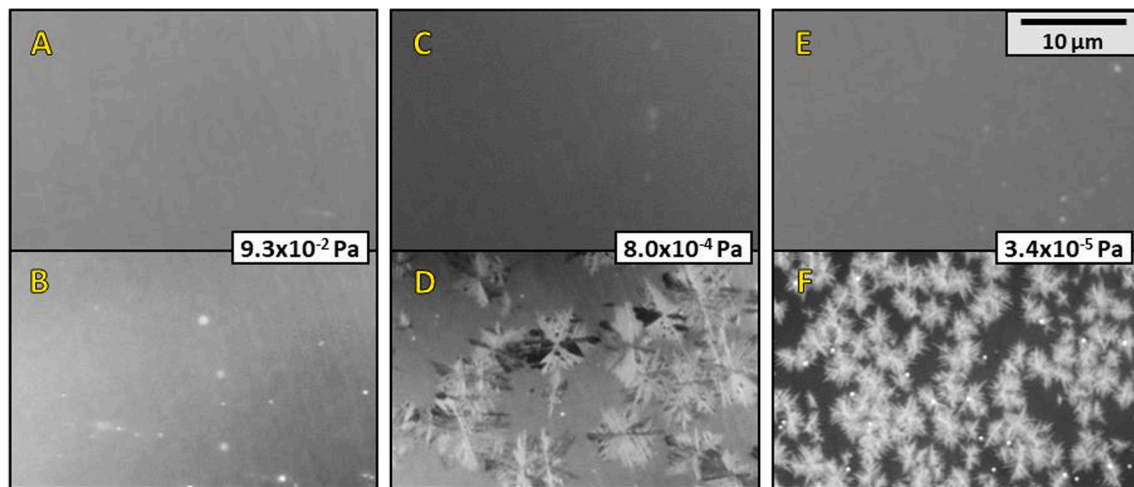


Fig. 1. Optical microscopy monochromatic light (460 nm) images corresponding to as-deposited EuO_x films (A, C, E), and to films annealed at 250 °C for 3 h (B, D, F). The films have been deposited at different background pressures of 9.3×10^{-2} Pa (A,B), 8.0×10^{-4} Pa (C,D) and 3.4×10^{-5} Pa (E,F).

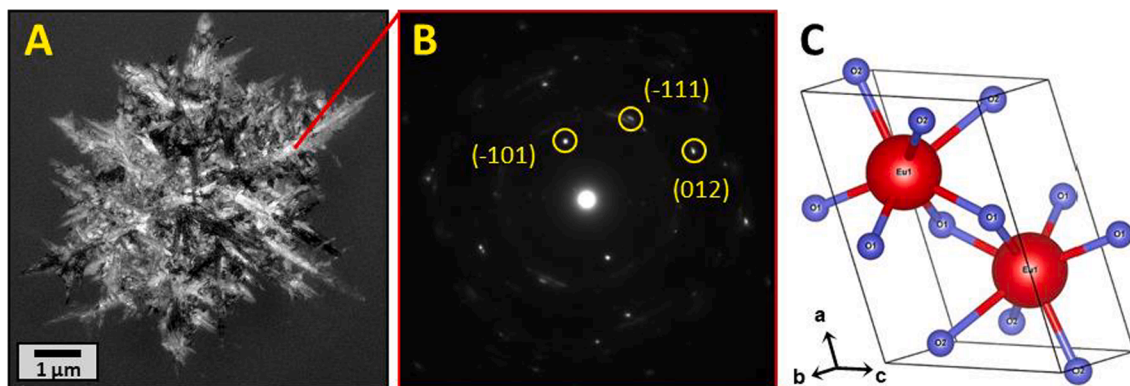


Fig. 2. (A) TEM image of a EuOOH crystallite obtained from the film deposited at 8.0×10^{-4} Pa and annealed at 250 °C for 3 h. (B) SAED pattern taken in an area inside the crystal. (C) Schematic representation of the EuOOH monoclinic unit cell. Image created by VESTA.[33].

Table 1

Crystallographic lattice parameters of the crystals synthesized in this work compared to other europium oxides structures.

Unit Cell Parameter (Å)	This work	Monoclinic EuOOH [34]	Cubic Eu_2O_3 [35]	Monoclinic Eu_2O_3 [36]	Cubic EuO [37]
<i>a</i>	6.15 ± 0.06	6.109	10.869	14.110	5.142
<i>b</i>	3.7 ± 0.1	3.748	10.869	3.602	5.142
<i>c</i>	4.2 ± 0.1	4.374	10.869	8.808	5.142

The minor lattice parameter deviations from those reported in the literature[34] (<0.05 Å for *a* and *b*, <0.2 Å for *c*) might be due to the intrinsic stress derived from the crystallization within the surrounding amorphous matrix and to the lattice mismatch with the substrate. [39,40].

We have further confirmed the crystalline structure of the annealed films through XRD analysis. Fig. 3 show XRD patterns corresponding to as-deposited films and to films after annealing at 250 °C (Supplementary material Fig. S1). The as-deposited films show a featureless pattern that indicates that the film is amorphous. The annealed films clearly show peaks corresponding to a crystalline structure. Its XRD pattern shows intense peaks at $2\theta = 22.0^\circ$, 28.5° and 51.5° along with other minor peaks ($2\theta = 15.5^\circ$, 31.5° , 33° , 41.5° , 47.1° , 51.8°). These peak positions

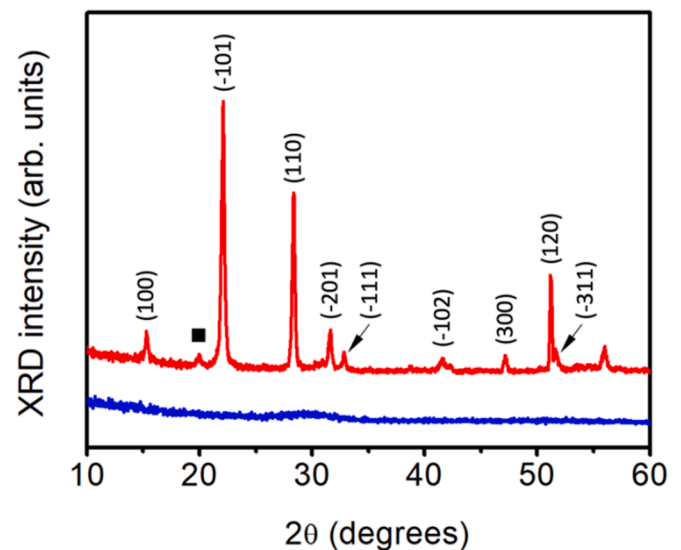


Fig. 3. XRD pattern for the films: (—) as-deposited, and (—) annealed at 250 °C for 3 h. The (■) square labeled peak correspond to an incipient Eu_2O_3 cubic phase. The crystallographic planes are indicated for each peak according to the JCPDS Card 018–510.

are in excellent agreement with that of the EuOOH monoclinic phase (JCPDS Card 018–510). The corresponding crystallographic plane is indicated for each peak in the figure. Finally, we also observe a small peak at 20° , which likely corresponds to an incipient Eu_2O_3 cubic phase. Increasing the annealing temperature up to 450°C leads to the complete transformation of the monoclinic EuOOH films into cubic Eu_2O_3 films (See [Supplementary material S2](#)). In the case of films annealed at 250°C , we have calculated the inter-reticular distances d_{hkl} (See [supplementary material S2](#)). The calculated d_{hkl} values are in excellent agreement with that of previous studies for bulk EuOOH. [34].

Fig. 4A shows the spectral dependence of the complex refractive index ($n = n + ik$) for both as-deposited and annealed films, where n is the refractive index and k is the absorption coefficient obtained from the ellipsometry measurements ([Supplementary material S3](#)). The refractive index optical functions have been modeled with a Cauchy function for the near infrared range, and with Cody-Lorentz and Gaussian oscillators to account for the absorption in the visible and ultraviolet spectral ranges. The model fittings are excellent ($\text{MSE} < 5$). The refractive index of as-deposited and annealed at 450°C (cubic Eu_2O_3) reference films are very similar, and in agreement with those reported previously for Eu_2O_3 thin films. [21] However, the refractive index of films annealed at 250°C (monoclinic EuOOH) is lower by about 0.1, which gives significant refractive index contrast to easily observe the crystalline stars in the optical microscope ([Fig. 1](#)). Concerning absorption, it is significantly higher in the ultraviolet range for as-deposited films than for the annealed films (monoclinic EuOOH and cubic Eu_2O_3 reference). This can be related to defects, most likely associated with oxygen vacancies that usually absorb in the UV. However, this absorption is highly reduced after annealing, and the extinction coefficient shows small values ($k < 1 \times 10^{-2}$) for both monoclinic EuOOH and cubic Eu_2O_3 reference crystalline films.

In order to understand the process of formation of EuOOH films upon annealing we have measured the transmission spectrum of different films in the infrared (IR) region (2300 to 3200 nm). The results are shown in [Fig. 4B](#), where we have included the IR transmission of a bare fused silica substrate as reference. The intense absorption band centered at 2720 nm (3675 cm^{-1}), which is also observed for the fused silica reference spectrum, corresponds to Si-O-H vibrations. [42] In addition to this band, the spectra show clear differences depending on the annealing temperature. The spectrum corresponding to as-deposited films shows a broad absorption band in the 2800 nm to 3150 nm

range that most likely corresponds to stretching vibrations of OH^- groups adsorbed during film fabrication and to H_2O absorbed after deposition. [17,43,44] The presence of a high concentration of OH^- groups in the films synthesized by PLD has been reported previously. [43,45,46] The high vacuum conditions used for deposition often lead to the formation of oxygen vacancies, [47,48] as suggested in this work by the optical characterization of the as-deposited films, which in turn may favor the water molecule dissociation in hydroxyl groups and their incorporation in these defect sites. [49] In the case of films annealed at 250°C , which leads to the formation of crystalline EuOOH films, the IR spectrum presents two clear differences. First, there is a sharp absorption peak centered at 2776 nm (3602 cm^{-1}), which can be assigned to the O-H stretching vibration mode in the EuOOH structure. [17,23,26,50] thus confirming the structural incorporation of OH^- groups. Second, the intensity of the IR absorption band in the range from 2800 nm to 3150 nm decreases significantly, thus suggesting a decrease on the concentration of adsorbed OH^- groups, that are either incorporated into the structure of the films or removed upon annealing at 250°C for 3 h. Finally, the spectrum of films annealed at 450°C that present a Eu_2O_3 cubic phase, does not show the sharp absorption at 2776 nm neither the broad absorption band in the 2800 nm to 3150 nm range. This confirms the total elimination of the OH^- groups from the structure. The structural evolution of the films with the annealing temperature is in good agreement with the evolution of the refractive index presented in [Fig. 4A](#). The formation of EuOOH at 250°C should lead to an overall decrease of the film density and, therefore, of its polarizability as it is experimentally observed. The subsequent annealing at 450°C , leads to a phase change from EuOOH to Eu_2O_3 cubic phase. As a result of the phase change the film density increases (from 6.51 g cm^{-3} to 7.42 g cm^{-3}) [34,51] and the refractive index increases as experimentally observed to reach the value expected for Eu_2O_3 films. [21] Furthermore, this is in agreement with our previous works that show that upon high temperature annealing ($500\text{--}800^\circ\text{C}$) stable Eu-oxides are formed. [15].

The evolution of the IR transmission of the films together with their TEM and XRD analysis allows us to provide a qualitative picture on the formation and decomposition of EuOOH upon annealing. We can consider as-deposited films as rare-earth hydrated oxides due their large concentration of weakly bonded OH^- groups and adsorbed H_2O molecules. [17,43,44] Upon annealing at 250°C partial dehydration of the films occurs, along with the change in the bonding of the OH^- groups within the formed crystal structure, which can be concluded by the

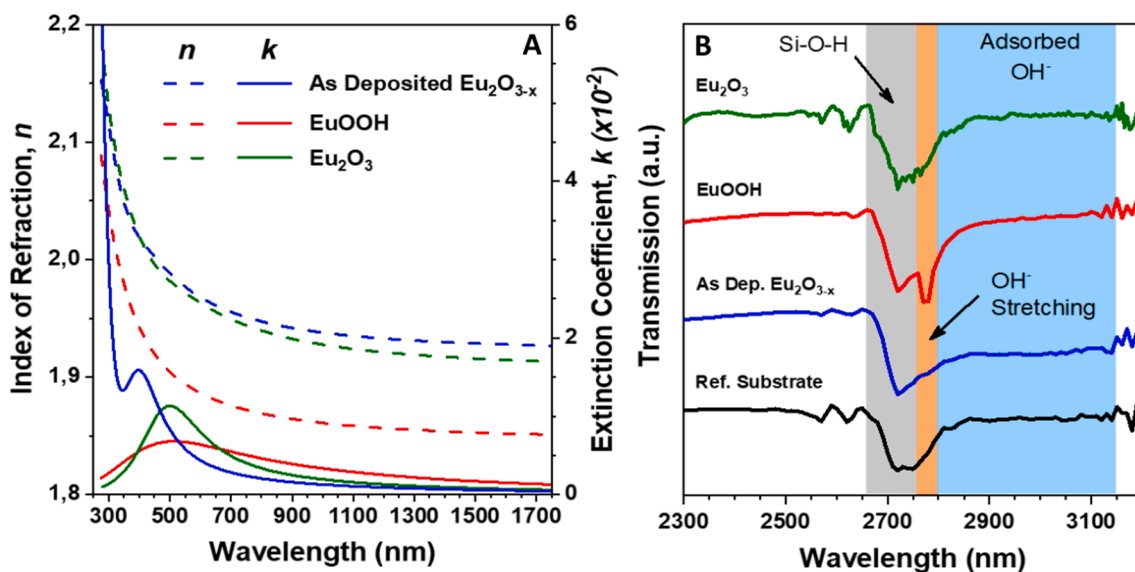


Fig. 4. (A) Refractive index, n (left axis), and absorption coefficient, k (right axis), determined from ellipsometry measurements, and (B) Transmission, T , measured in the infrared for films prepared at $P = 8.0 \times 10^{-4}$ Pa after annealing at different temperatures: as-deposited, annealed at 250°C for 3 h (EuOOH), and annealed at 450°C for 1 h (Eu_2O_3).

appearance of the characteristic absorption peak at 3602 cm^{-1} associated to OH^- stretching vibrations in EuOOH (Fig. 4B). This evolution upon annealing can be explained by the fact that rare-earth hydrated oxides are less stable than the corresponding oxyhydroxides.[52] The results thus suggest that after the annealing the OH^- groups are incorporated into the structure of the films, and this process is correlated to their crystallization and formation of the EuOOH (Fig. 1D, F). Further increase of the annealing temperature at 450°C induces the decomposition of the EuOOH in the films to form Eu_2O_3 . The temperature values at which we have observed the formation (T_f) at 250°C , and decomposition (T_d), at 450°C , of our EuOOH films are in very good agreement with those previously reported for the case of bulk ($T_f = 225\text{--}300^\circ\text{C}$, and $T_d = 425\text{--}465^\circ\text{C}$), and nanorods ($T_f = 300^\circ\text{C}$ (f) and $T_d > 350^\circ\text{C}$). [23,25,26,53].

Finally, to further characterize the structure of the monoclinic EuOOH synthesized films we have performed micro-Raman analysis. However, we must emphasize that we have found no literature information of the vibrational modes, neither for infrared nor for Raman spectra, for the monoclinic EuOOH phase. Moreover, RE-oxyhydroxides are isostructural and analogous to YOOH , crystallizing with a C_{2h} point group and a small primitive cell with $Z = 2$. [52,54–57] It should be noted that the position of the hydrogen ions cannot be obtained from electron diffraction or XRD studies, thus the group analysis of the vibration modes is performed considering the OH^- as a unit with the location of its oxygen. In this approximation, the total number of vibration modes is $18: 6A_g + 3A_u + 3B_g + 6B_u$, all of which are non-degenerated. Among these, $A_u + 2B_u$ are the three acoustic modes, $2A_u + 4B_u$ are the six infrared active modes, and $6A_g + 3B_g$ are the nine Raman active modes. The Eu, O1 and O2 ions are located at 2e sites so all types of ions participate in the Raman phonons similarly. In backscattering geometry, the B_g modes cannot be detected if the incident direction coincides with the z-axis of the crystal. This is not the present case since the films are formed by crystallites with different orientations within the laser spot size of $\sim 0.8\text{ }\mu\text{m}$ in diameter (see Fig. 1D,F), therefore the nine active Raman modes are, in principle, observable in

our experimental configuration.

Fig. 5A and B shows representative Raman spectra of the monoclinic EuOOH films and of the cubic Eu_2O_3 reference films, respectively. The spectra show narrow peaks for both films in agreement with their crystalline structure. All the experimentally observed Raman peaks have been included in Table 2, along with the previously reported data in the literature for cubic and monoclinic Eu_2O_3 phases.[57,58] We will analyze first the data for the case of the Eu_2O_3 reference films because this material is well known and Raman spectra have been previously reported for its phases. We observe a very good correlation with

Table 2

Frequencies of the phonon modes measured by Raman spectroscopy corresponding to the monoclinic (monocl.) EuOOH and cubic Eu_2O_3 films along with literature data for the monoclinic and cubic Eu_2O_3 phases.

This work		Literature data	
Monocl. EuOOH (cm^{-1})	Cubic Eu_2O_3 (cm^{-1})	Monocl. Eu_2O_3 [58] (cm^{-1})	Cubic Eu_2O_3 [57] (cm^{-1})
120	116	110	109
133		116	119
		152	134
		176	145
195			175
		218	
236		246	
	280	259	
	332	285	289
332			339
348.5			
		374	
378		377	
			385
406	416	394	
		413	
		424	425
466		465	

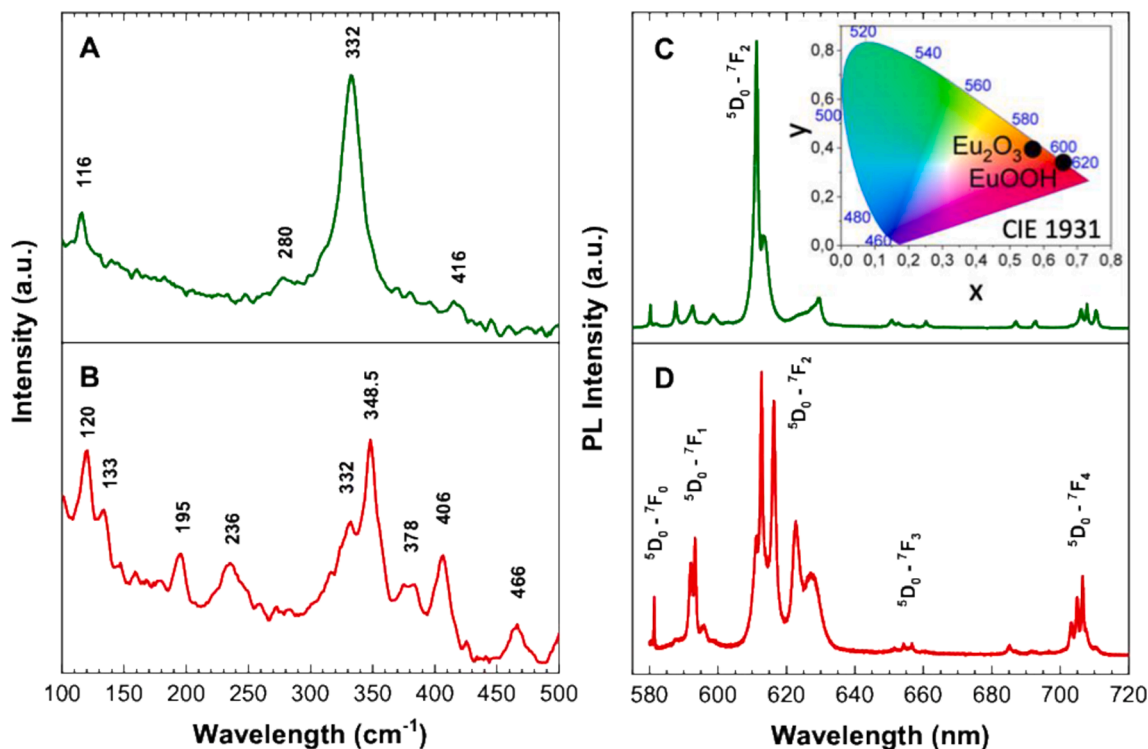


Fig. 5. Raman (A,B) and micro-PL (C,D) normalized spectra ($\lambda_{\text{exc}} = 488\text{ nm}$) of the cubic Eu_2O_3 (A,C) and monoclinic EuOOH (B,D) films. The inset in C shows the CIE 1931 diagram chromatic coordinates for both types of films.

previous published results, in particular, the most intense peak located at 332 cm^{-1} is associated with the 339 cm^{-1} peak which is due to oxygen vibrations along the oxygen chains.[59] However, as shown in Table 2, all the modes show a small frequency reduction compared to those previously reported. This softening can be due to the presence of oxygen vacancies in our cubic Eu_2O_3 reference films;[59] this being in good agreement with the observed absorption peak in the k spectrum for cubic Eu_2O_3 films (Fig. 4A). Having the results of the reference films in mind we analyze now the Raman spectrum corresponding to monoclinic EuOOH films (Fig. 5B). The spectrum shows nine Raman peaks that are included in Table 2, which is in good agreement with the vibrational modes predicted by the group analysis performed above and with the known structural properties of the EuOOH phase.

The frequency of vibrational modes observed in the case of monoclinic EuOOH are in the range from 110 to 470 cm^{-1} , which corresponds to the frequency range of the modes reported for cubic and monoclinic Eu_2O_3 as it is shown in Table 2.[58–60] This coincidence is expected since the vibrations are originated by the same ions (Eu and O) for all the studied compounds and different phases, and moreover, the Eu-O bond distances are similar (average Eu-O bonds for first neighbors are around $2.3 - 2.5\text{ Å}$ in all cases). Finally, It is interesting to remark that the measured spectrum for the monoclinic EuOOH phase shows clear differences compared to those of the cubic (Fig. 5A) and monoclinic Eu_2O_3 phases.[60] Characteristic peaks at 133 , 195 , 236 , 348.5 , 378 and 466 cm^{-1} have been clearly identified, while, the 120 and 332 cm^{-1} peaks, also observed in our cubic Eu_2O_3 reference films, might be partially due to the presence of a coexisting incipient cubic Eu_2O_3 phase in the EuOOH film as suggested by the XRD analysis (Fig. 3).

Fig. 5C and D compare the micro-PL spectra of EuOOH films with of cubic Eu_2O_3 reference films. The assignments of the transition manifolds have been indicated in the figures; they correspond to intra-4f transitions of the Eu^{3+} ion. The micro-PL spectrum obtained for the EuOOH film (Fig. 4D) shows several narrow peaks pointing to high crystallinity. The emission is attributed to the $^5\text{D}_0 \rightarrow ^7\text{F}_J$ ($J = 0-4$) transitions of Eu^{3+} ions in the monoclinic phase, as reported for bulk EuOOH powder crystals.[19,26] The emission color is in the red region due the higher intensity of the electric dipolar transition $^5\text{D}_0 \rightarrow ^7\text{F}_2$ (612.7 , 616.3 , 622.7 and 627.3 nm). We observe several emission peaks due to the splitting of the optical transitions as a result of the low symmetry of the crystalline field in the monoclinic phase. In this way, the low point of symmetry (C_2) of the Eu^{3+} ion in the EuOOH structure allows the $^5\text{D}_0 \rightarrow ^7\text{F}_0$ transition.[55] The single weak line $^5\text{D}_0 \rightarrow ^7\text{F}_0$ transition at 581.3 nm , indicates a unique environment for the Eu^{3+} in the EuOOH . All observed emission peaks from the Eu^{3+} in EuOOH are purely electronic and have no contribution of vibronically induced transitions.[19] In contrast, the film emission changes significantly upon annealing at 450 °C . We observe a strong increase of the emission intensity by a factor four of the hypersensitive $^5\text{D}_0 \rightarrow ^7\text{F}_2$ transition (611.3 , 613.3 and 629.4 nm) that dominates the spectrum. This behavior is characteristic of a cubic-phase Eu_2O_3 (Fig. 5C) in which there are two possible crystallographic sites for the Eu^{3+} ions, a high symmetry (S_6) and a low symmetry (C_2) sites that are responsible for the all the observed peaks.[61,62] In particular, the observed emission enhancement with respect to EuOOH PL spectrum is related to the energy transfer from the Eu^{3+} ions occupying S_6 sites to C_2 sites.[63] We have finally calculated the chromatic coordinates (CIE 1931) corresponding to the visible color photoluminescence emission for the EuOOH films ($x = 0.66$, $y = 0.34$) and compared to that of cubic- Eu_2O_3 reference films ($x = 0.57$, $y = 0.39$), the results are displayed in the inset of Fig. 5C. EuOOH films show a high purity red color emission, whereas cubic Eu_2O_3 reference films show a small displacement toward orange-red color. This interesting phenomenon of a well differentiated emission of the Eu^{3+} ion depending on the crystalline environment can be successfully used to tune the emission color of the films as shown in previous works,[21,22] and it is relevant for security applications as it can be implemented in anti-counterfeiting technologies.

4. Conclusions

Crystalline and optically active Eu oxyhydroxide (EuOOH) thin films have been successfully fabricated by PLD in vacuum. The crystal formation depends critically on the background pressure during deposition, and it has been found at pressures lower than $1.0 \times 10^{-3}\text{ Pa}$ followed by annealing at low temperatures (250 °C) in air. The formation of the EuOOH monoclinic phase has been unambiguously identified by TEM and XRD analysis. As-deposited films are amorphous and have a large concentration of weakly bonded OH^- groups and absorbed water. Subsequent annealing at 250 °C induces their crystallization and a partial dehydration, along with the introduction of OH^- groups into their network structure that leads to formation of monoclinic EuOOH films. Further annealing at 450 °C thermally decomposes them into cubic Eu_2O_3 films. The complex refractive index in the visible and near infrared range of the monoclinic EuOOH films has been determined by spectroscopic ellipsometry. These films show a characteristic refractive index that is lower, both real and imaginary parts, than that of europium oxides, with a high transparency in the $275\text{--}1750\text{ nm}$ range. EuOOH has a high purity red photoluminescence emission with narrow peaks attributed to the $^5\text{D}_0 \rightarrow ^7\text{F}_J$ ($J = 0\text{--}4$) transitions of the Eu^{3+} ions in unique site of $P2_1/m$ monoclinic structure. Finally, we report the characteristic vibrational modes of monoclinic EuOOH in the 110 to 470 cm^{-1} range as measured by Raman spectroscopy. This measured spectrum will allow an easy identification of the monoclinic EuOOH phase in the future, clearly differentiating it from other Europium oxygen-hydrogen compounds. We believe that these novel EuOOH films that have been successfully prepared both on Si and fused silica substrates show excellent optical properties, and they are promising for their integration in solid state optoelectronic components and devices. Future work will focus on improving the efficiency of the fabrication process by testing if the process could be made single step by PLD in oxygen / hydrogen mixed atmosphere or water vapor.

Declaration of Competing Interest

The authors declare that they have no known competing financial interests or personal relationships that could have appeared to influence the work reported in this paper.

Data availability

Data will be made available on request.

Acknowledgements

This work was funded by the Spanish Research Agency (AEI, Ministry of Research and Innovation) and the European Regional Development Fund (ERDF) under grants RTI2018-096498-B-I00, RTI2018-101020-B-I00, RTI2018-096918-B-C41 and PID2021-123190OB-I00; by the CSIC (PIE-202050E195 and project 2021AEP128IO); by the Regional Government of Madrid through TECHNOfUSIÓN(III)CM (S2018/EMT-4437); and by Comunidad de Madrid (Spain) multiannual agreement with UCM3M, “Excelencia para el Profesorado Universitario” (EPUC3M14) - Fifth regional research plan 2016-2020. The work of A. Caño was partially supported by the Autonomous Community of Madrid and the European Social Fund (PEJD-2019-PRE/TIC-16082).

Appendix A. Supplementary data

Supplementary data to this article can be found online at <https://doi.org/10.1016/j.apsusc.2023.158236>.

References

- [1] G. Liu, B. Jacquier (Eds.), *Spectroscopic Properties of Rare Earths in Optical Materials*, Springer, Berlin Heidelberg, 2005.
- [2] J. Qiao, S. Zhang, X. Zhou, W. Chen, R. Gautier, Z. Xia, *Adv. Mater.* 34 (2022) 2201887.
- [3] Z. Zeng, B. Huang, X. Wang, L. Lu, Q. Lu, M. Sun, T. Wu, T. Ma, J. Xu, Y. Xu, S. Wang, Y. Du, C.H. Yan, *Adv. Mater.* 32 (2020) 2004506.
- [4] Z. Xiao, R. Serna, C.N. Afonso, I. Vickridge, *Appl. Phys. Lett.* 87 (2005), 111103.
- [5] P. Gomez-Rodriguez, E. Soria, Y. Jin, A. Caño, I. Llorente, A. Cuadrado, A. Mariscal-Jiménez, A.K. Petford-Long, R. Serna, J. Gonzalo, *Nanophotonics* 10 (2021) 3995.
- [6] I. Camps, A. Mariscal, L. Calvo-Barrio, R. Serna, *Phys. Status Solidi Appl. Mater. Sci.* 215 (2018) 1.
- [7] I. Camps, A. Mariscal-Jiménez, R. Serna, *Appl. Surf. Sci.* 613 (2023) 1.
- [8] R.F. D'Vries, S. Álvarez-García, N. Snejkó, L.E. Bausá, E. Gutiérrez-Puebla, A. De Andrés, M.A. Monge, *J. Mater. Chem. C* 1 (2013) 6316.
- [9] R.I. Guar, C.J. Tighe, J. Muir, J.T. Kittler, M. Wodjak, A.J. Kenyon, J.A. Darr, *RSC Adv.* 2 (2012) 10037.
- [10] K.-L. Wong, G.-L. Law, M.B. Murphy, P.A. Tanner, W.-T. Wong, P.-K.-S. Lam, M.-H.-W. Lam, *Inorg. Chem.* 47 (2008) 5190.
- [11] S. Ben-David Makhlef, R. Arnon, C.R. Patra, D. Mukhopadhyay, A. Gedanken, P. Mukherjee, H. Breitbart, *J. Phys. Chem. C* 112 (2008) 12801.
- [12] E. Ximenes, A. Benayas, D. Jaque, R. Marin, *ACS Nano* 2021 (1917) 15.
- [13] T. Kataoka, T. Hashimoto, S. Samitsu, Z. Liu, M. Tagaya, *A.C.S. Appl. Nano Mater.* 5 (2022) 2305.
- [14] D. Jaque, C. Richard, B. Viana, K. Soga, X. Liu, J. García Solé, *Adv. Opt. Photon.* 8 (2016) 1.
- [15] F. Gándara, A. De Andrés, B. Gómez-Lor, E. Gutiérrez-Puebla, M. Iglesias, M. A. Monge, D.M. Proserpio, N. Snejkó, *Cryst. Growth Des.* 8 (2008) 378.
- [16] S. Cornelius, G. Colombi, F. Nafezarefi, H. Schreuders, R. Heller, F. Munnik, B. Dam, *J. Phys. Chem. Lett.* 10 (2019) 1342.
- [17] S.K. Hussain, G. Nagaraju, E. Pavitra, G. Seeta Rama Raju, J.S. Yu, *CrstEngComm* 17 (2015) 9431.
- [18] H. Samata, D. Itakura, S. Imanaka, T.C. Ozawa, *J. Mater. Sci. Chem. Eng.* 02 (2014) 23.
- [19] J. Hölsä, T. Leskelä, M. Leskelä, *Inorg. Chem.* 24 (1985) 1539.
- [20] A. Quesada, A. del Campo, J.F. Fernández, *J. Eur. Ceram. Soc.* 2014 (1803) 34.
- [21] A. Mariscal, A. Quesada, I. Camps, F.J. Palomares, J.F. Fernández, R. Serna, *Appl. Surf. Sci.* 374 (2016) 71.
- [22] A. Mariscal-Jiménez, A. Tarazaga Martín-Luengo, B. Galiana, C. Ballesteros, A. Bonanni, J. Martín-Sánchez, R. Serna, *J. Phys. Chem. C* 124 (2020) 15434.
- [23] J.G. Kang, Y. Jung, B.K. Min, Y. Sohn, *Appl. Surf. Sci.* 314 (2014) 158.
- [24] D. Zhang, T. Yan, L. Shi, H. Li, J.F. Chiang, *J. Alloy. Compd.* 506 (2010) 446.
- [25] R.C. Rau, W.J. Glover, *J. Am. Ceram. Soc.* 47 (1964) 382.
- [26] H.G. Brittain, J.V. Posluszny, *Thermochim. Acta* 118 (1987) 25.
- [27] J. Winczewski, M. Herrera, C. Gabriel, I. Izeddin, S. Gabel, B. Merle, A. Susarrey Arce, H. Gardeniers, *Adv. Opt. Mater.* (2022) 2102758.
- [28] C.N. Afonso, R. Serna, J.M. Ballesteros, A.K. Petford-Long, R.C. Doole, *Appl. Surf. Sci.* (1998) 127–129.
- [29] R. Serna, A. Suárez-García, C.N. Afonso, D. Babonneau, *Nanotechnology* 17 (2006) 4588.
- [30] G. Colombi, T. De Krom, D. Chaykina, S. Cornelius, S.W.H. Eijt, B. Dam, *ACS Photonics* 8 (2021) 709.
- [31] C.N. Afonso, J. Gonzalo, R. Serna, J. Solís, *Springer Ser. Opt. Sci.* (2007) 315–338.
- [32] J. Gonzalo, R. Serna, J.M. Requejo, J. Solís, C.N. Afonso, A. Naudon, *Appl. Surf. Sci.* 154 (2000) 449.
- [33] K. Momma, F. Izumi, *J. Appl. Cryst.* 44 (2011) 1272.
- [34] H. Bärnighausen, *Acta Crystallogr.* 19 (1965) 1047.
- [35] H. Kohlmann, C. Hein, R. Kautenburger, T.C. Hansen, C. Ritter, S. Doyle, *Zeitschrift für Krist. - Cryst. Mater.* 231 (2016) 517.
- [36] H.L. Yakel, *Acta Crystallogr. Sect. B Struct. Crystallogr. Cryst. Chem.* 35 (1979) 564.
- [37] D. Taylor, *Trans. Br. Ceram. Soc.* 83 (1984) 92.
- [38] H. Samata, N. Wada, T.C. Ozawa, *J. Rare Earths* 33 (2015) 177.
- [39] F.O. Adurodija, H. Izumi, T. Ishihara, H. Yoshioka, M. Motoyama, *J. Mater. Sci. Mater. Electron.* 12 (2001) 57.
- [40] Y.C. Zhou, Z.Y. Yang, X.J. Zheng, *Surf. Coatings Technol.* 162 (2003) 202.
- [42] B.A. Gawel, A. Ulvensen, K. Łukaszuk, B. Arstad, A.M.F. Muggerud, A. Erbe, *RSC Adv.* 10 (2020) 29018.
- [43] R. Morea, A. Miguel, T.T. Fernandez, B. Maté, F.J. Ferrer, C. Maffiotte, J. Fernandez, R. Balda, J. Gonzalo, *J. Lumin.* 170 (2016) 778.
- [44] R.D.L. Gaspar, I.O. Mazali, F.A. Sigoli, *Colloids Surfaces A Physicochem. Eng. Asp.* 367 (2010) 155.
- [45] M. Irannejad, G. Jose, A. Jha, D.P. Steenson, *Opt. Mater. (Amst.)* 33 (2010) 215.
- [46] M. Irannejad, G. Jose, P. Steenson, A. Jha, *Opt. Mater. (Amst.)* 34 (2012) 1272.
- [47] J.A. Chaos, J. Gonzalo, C.N. Afonso, J. Perrière, M.T. García-González, *Appl. Phys. A Mater. Sci. Process.* 72 (2001) 705.
- [48] A. Mariscal, A. Quesada, A. Tarazaga Martín-Luengo, M.A. García, A. Bonanni, J. F. Fernández, R. Serna, *Appl. Surf. Sci.* 456 (2018) 980.
- [49] X. Deng, T. Herranz, C. Weis, H. Bluhm, M. Salmeron, *J. Phys. Chem. C* 112 (2008) 9668.
- [50] B.I. Swanson, C. Machell, G.W. Beall, W.O. Milligan, *J. Inorg. Nucl. Chem.* 40 (1978) 694.
- [51] D.R. Lide, *CRC Handbook of Chemistry and Physics*, 88th Edition, Taylor & Francis, 2007.
- [52] S. Yang, M. Powell, J.W. Kolis, A. Navrotsky, *J. Solid State Chem.* 287 (2020), 121344.
- [53] O. Yamamoto, Y. Takeda, R. Kanno, M. Fushimi, *Solid State Ion.* 17 (1985) 107.
- [54] H. Samata, D. Kimura, Y. Saeki, Y. Nagata, T.C. Ozawa, *J. Cryst. Growth* 304 (2007) 448.
- [55] J. Hölsä, *J. Phys. Chem.* 94 (1990) 4835.
- [56] A.N. Christensen, A. Kjekshus, T. Skansen, J. Brunvoll, M. Hinton, *Acta Chem. Scand.* 19 (1965) 1391.
- [57] P.V. Klevtsov, R.F. Klevtsova, L.P. Sheina, *Zhurnal Strukturalnoi Khimii* 5 (1964) 583.
- [58] J. Łażewski, M. Sternik, P.T. Jochym, J. Kalt, S. Stankov, A.I. Chumakov, J. Göttlicher, R. Rüffer, T. Baumbach, P. Piekarz, *Inorg. Chem.* 60 (2021) 9571.
- [59] M.V. Abrashev, N.D. Todorov, J. Geshev, *J. Appl. Phys.* 116 (2014), 103508.
- [60] J. Gouteron, D. Michel, A.M. Lejus, J. Zarembowitch, *J. Solid State Chem.* 38 (1981) 288.
- [61] E. Antic-Fidancev, J. Hölsä, M. Lastusaari, *J. Alloy. Compd.* 341 (2002) 82.
- [62] G.B.F. Bosco, L.R. Tessler, *Opt. Mater. X* 2 (2019), 100028.
- [63] P. Packiyaraj, P. Thangadurai, *J. Lumin.* 145 (2014) 997.